nature neuroscience

Distinct contributions of $Na_v1.6$ and $Na_v1.2$ in action potential initiation and backpropagation

Wenqin Hu, Cuiping Tian, Tun Li, Mingpo Yang, Han Hou & Yousheng Shu

The distal end of the axon initial segment (AIS) is the preferred site for action potential initiation in cortical pyramidal neurons because of its high Na^+ channel density. However, it is not clear why action potentials are not initiated at the proximal AIS, which has a similarly high Na^+ channel density. We found that low-threshold $Na_v1.6$ and high-threshold $Na_v1.2$ channels preferentially accumulate at the distal and proximal AIS, respectively, and have distinct functions in action potential initiation and backpropagation. Patch-clamp recording from the axon cut end of pyramidal neurons in the rat prefrontal cortex revealed a high density of Na^+ current and a progressive reduction in the half-activation voltage (up to 14 mV) with increasing distance from the soma at the AIS. Further modeling studies and simultaneous somatic and axonal recordings showed that distal $Na_v1.6$ promotes action potential initiation, whereas proximal $Na_v1.2$ promotes its backpropagation to the soma.

Although action potentials can be independently initiated at many sites in a neuron[1–7], pioneering studies in spinal motorneurons[8–11] and recent works in cortical pyramidal neurons[6,7,12–14] have demonstrated that the AIS has the lowest threshold for action potential initiation, up to 15 mV lower than that at the soma[8–10,14], as a result of a high concentration of Na^+ channels[4,15–17]. Further studies in layer 5 pyramidal neurons have shown that the action potential initiation site is located in the distal region of the AIS, a specialized subcellular domain targeted by certain types of K^+ channels[18–21] and innervated by axo-axonic GABAergic interneurons[19,22].

Because immunostaining studies and patch-clamp recordings have indicated a similar density of Na^+ channels along the length of the AIS[3,23,24], it has been unclear why action potentials are preferentially initiated at the distal rather than at the proximal region of the AIS. One explanation could be that the biophysical property of Na^+ channels may differ in the proximal versus distal compartments. Indeed, initial cell-attached and outside-out patch recordings have revealed a ~7-mV hyperpolarizing shift in the activation curve of Na^+ channels at the AIS relative to that at the soma[3]. Recent immunostaining studies on different neuronal types have demonstrated that the Na^+ channel subtypes may be specifically targeted to different AIS regions[18,24–27]. Because Na^+ channel subtypes have different activation thresholds[28], their subcellular distribution and density at the AIS may contribute to the action potential initiation and regulation[25,29–31]. Thus, a full resolution of the role of density versus voltage-dependent properties of Na^+ channels at the AIS requires the mapping of the distribution of Na^+ channel subtypes and direct recording from the axonal membrane at both the proximal and the distal regions of the AIS.

We carried out immunostaining for Na^+ channel subtypes and patch-clamp recordings from giant patches (somatic nucleated patches and isolated axon blebs), as well as regular outside-out patches, to investigate the distribution and biophysical properties of Na^+ channels in the somatic and AIS/axonal membrane. Our results provide a quantitative description of the selective accumulation of $Na_v1.6$ and $Na_v1.2$ channels at the distal and proximal AIS, respectively. Further computational modeling and simultaneous recordings from the soma and the axon indicated that this selective accumulation of $Na_v1.6$ at the distal AIS determines the action potential initiation site, whereas accumulation of $Na_v1.2$ at the proximal AIS promotes action potential propagation to the soma and sets the action potential threshold of the somatodendritic region of the neuron.

RESULTS

Differential distribution of Na^+ channel subtypes at AIS

We first performed immunostaining of layer 5 pyramidal neurons of the rat prefrontal cortex to map the distribution of Na^+ channel subtypes and the Na^+ channel–associated protein ankyrin-G (AnkG), which is known to accumulate at the AIS (**Fig. 1**). We found a differential distribution of $Na_v1.2$ and $Na_v1.6$ at the proximal and distal AIS, respectively (**Fig. 1a**,**b**). Quantitative measurements of the immunofluorescence intensity for a large population of neurons in 16-μm-thick cortical sections showed a polarized distribution of $Na_v1.2$ and $Na_v1.6$ at the AIS (**Fig. 1a**,**b**). Further immunostaining of 100-μm-thick sections showed a peak in the density of $Na_v1.6$ channels between 30 and 50 μm from the soma (**Supplementary Fig. 1**), corresponding to the action potential initiation zone that was previously identified[6,7,12,13]. The length of the AIS, as reflected by AnkG staining, extended up to 70 μm from the soma.

To examine the density of total Na^+ channels, we stained the AIS with a pan-alpha Na^+ channel antibody (Pan-Na_v), which recognizes

Institute of Neuroscience, State Key Laboratory of Neuroscience, Shanghai Institutes for Biological Sciences, Chinese Academy of Sciences, Shanghai, China. Correspondence should be addressed to Y.S. (shu@ion.ac.cn).

Received 5 December 2008; accepted 27 May 2009; published online 26 July 2009; doi:10.1038/nn.2359

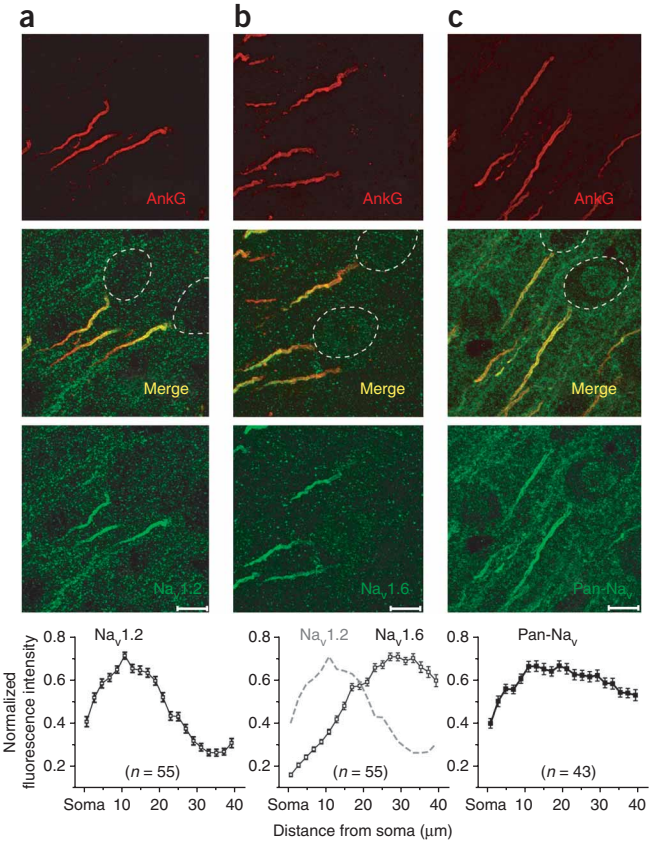

Figure 1 Polarized distribution of Na^+ channel subtypes. (**a**) Antibody staining for AnkG (red) and $Na_V1.2$ (green) in the rat prefrontal cortex. Note that the proximal AIS had strong staining for $Na_V1.2$. (**b**) Double staining for AnkG and $Na_V1.6$ (green). Note that the distal region of the AIS was heavily stained. (**c**) Double staining for AnkG and Pan-Na_V (green). Plots of the averaged (± s.e.m.) fluorescence intensity (see Online Methods) as a function of distance from the soma at the AIS are shown for **a**–**c**. Images are projections of confocal *z* stacks. Scale bars represent 10 μm. Error bars represent s.e.m.

both $Na_V1.2$ and $Na_V1.6$ channels. Consistent with previous findings, we observed strong Pan-Na_V immunoreactivity at the AIS, with a peak distribution between 10 and 20 μm (**Fig. 1c**), corresponding to the region of $Na_V1.2$ accumulation. Although immunoreactivity was undetectable in the somatic membrane, electrophysiological recordings in the following experiments indicated that high-threshold Na^+ channels were present in the soma (see below).

Na^+ current density is highest at the AIS

We next carried out voltage-clamp recordings in layer 5 pyramidal neurons to examine the density and voltage-dependent property of Na^+ currents along the somato-axonal axis. These neurons had an initial unmyelinated axon segment that was up to 300 μm long[13]. We obtained outside-out patches from the soma and the blebs (3–6 μm in diameter) formed at the axon cut end during slicing procedures[13,21,32].

In contrast with previous findings[2,3], we found that the amplitude of the transient Na^+ currents progressively increased from 0 to 30 μm from the soma, reaching an average value of 923 ± 85 pA ($n = 23$) at 30–70 μm (**Fig. 2a–c**), the distal AIS region corresponding to the action potential initiation zone[6,7,13,33]. Furthermore, the Na^+ current amplitude at the unmyelinated axonal regions distal to the AIS (>70 μm), although lower than that at the distal AIS, was still much higher than that found at the soma (**Fig. 2a–c**). Consistent with previous reports[2,3,23], the somatic Na^+ currents recorded in the regular outside-out patches were small (26.9 ± 4.7 pA, $n = 17$; **Fig. 2a–c**). In somatic nucleated patches (**Fig. 2d**), we observed much larger Na^+ currents (670 ± 54 pA, $n = 34$). In addition to recording from excised outside-out patch, we also recorded currents from isolated axon blebs and compared the data with those obtained from somatic nucleated patches. The peak Na^+ currents from isolated blebs varied from 0.5 to 3.5 nA (**Fig. 2d,e**). Normalization by the bleb surface area yielded a current density of 25.4 ± 2.3 pA μm^{-2} ($n = 11$; **Fig. 2e**), which was ~19-fold higher than that of somatic nucleated patches (1.5 ± 0.1 pA μm^{-2}, $n = 34$). Together, these results provide direct electrophysiological evidence for the highly clustered distribution of Na^+ channels at the AIS, as predicted previously by computational modeling[4,17] and shown by immunostaining studies[12,18,19,25,34].

Distal axonal Na^+ channels have the lowest threshold

Examination of the voltage-dependent properties of Na^+ currents revealed that Na^+ channels in the distal AIS and axonal membrane (50–500 μm from soma) had an average activation threshold of −55.5 ± 0.8 mV ($n = 14$, average distance 77.8 ± 10.1 μm) and complete activation at around −20 mV, whereas somatic Na^+ channels had an activation threshold of −42.7 ± 1.1 mV ($n = 11$) and complete activation at −10 to −5 mV (**Fig. 3a,b**). Fitting the activation curves using Boltzmann equation yielded the half-activation voltages ($V_{1/2}$) and slopes (axon: $V_{1/2} = -43.9 \pm 1.3$ mV, $k = 5.7 \pm 0.2$; soma: $V_{1/2} = -29.7 \pm 1.0$ mV, $k = 5.8 \pm 0.2$). There was no significant difference between the slopes ($P = 0.12$), but the activation curve for

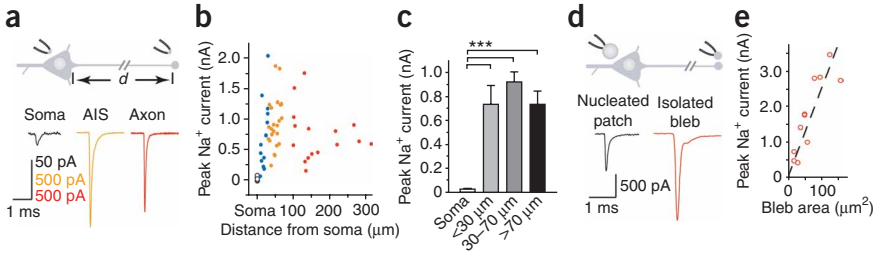

Figure 2 Estimates of Na^+ channel density at the soma and the axon with regular and giant outside-out patch recording. (**a**) Top, schematic diagram of the outside-out recording from patches excised from the soma and axon blebs. Bottom, examples of peak Na^+ current evoked by step depolarizations (30 ms) from a holding potential of −100 to +20 mV in outside-out patches obtained from the soma (black), AIS (orange, distance (d) = 39 μm) and axon (red, d = 265 μm). (**b**) Plot of peak Na^+ current in somatic and axonal outside-out patches with varying distances from the soma, indicating a peak distribution of Na^+ currents at the distal AIS. (**c**) Average amplitude (± s.e.m.) of the peak Na^+ current obtained from the soma and different compartments of the axon. Error bars represent s.e.m. *** indicates $P < 0.001$. (**d**) Top, schematic diagram of the giant outside-out patch recordings: nucleated patch and isolated bleb recording. Bottom, examples of peak Na^+ current in nucleated patch (black) and isolated bleb (red, >50 μm). (**e**) Plot of peak Na^+ current as a function of bleb surface area. The dashed line represents the linear regression fit.

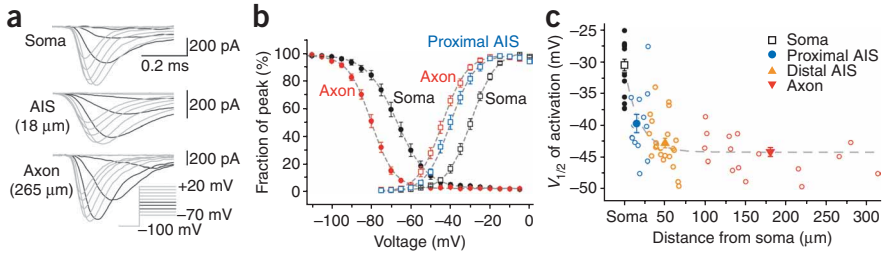

Figure 3 Comparison of voltage dependence of somatic and axonal Na^+ currents. (**a**) Representative families of Na^+ currents evoked by step depolarizations (inset) at soma (nucleated patches), AIS and axon (regular outside-out patches). (**b**) Activation and availability curves for somatic and axonal (>50 μm from the soma) Na^+ current. The activation curve for proximal-AIS Na^+ current (<30 μm) was inserted for comparison. The values were normalized to the peak current and then averaged (± s.e.m.) between different neurons. These data could be well fitted with Boltzmann equations (dashed lines). Soma, proximal AIS and axon indicate the results obtained from somatic nucleated patches, proximal AIS and axonal outside-out patches, respectively. (**c**) The $V_{1/2}$ of activation was plotted as a function of recording distances from the soma. Single exponential fit (dashed line) revealed a steep reduction in $V_{1/2}$ with a length constant of 18.4 ± 5.1 μm ($n = 53$). The averaged $V_{1/2}$ (± s.e.m.) for different compartments are shown. Error bars represent s.e.m.

axonal currents showed a hyperpolarizing shift of ~14 mV (**Fig. 3b**), a value twice that reported previously[3,23]. The half-inactivation voltages showed a similar shift (axon: −80.0 ± 1.0 mV, $n = 13$; soma: −67.0 ± 1.7 mV, $n = 11$), whereas the slopes were 5.4 ± 0.2 and 7.1 ± 0.3 for axonal and somatic Na^+ currents, respectively (**Fig. 3b**).

We next examined the properties of Na^+ channels in outside-out patches excised from axon blebs at various distances from the soma (8–310 μm; **Fig. 3c**). $V_{1/2}$ showed a gradual reduction (hyperpolarization) with increasing distance from the soma (8–50 μm) and reached a relatively steady value in the axon regions beyond the AIS (**Fig. 3c**). On the basis of these data and our immunostaining results, we concluded that the Na^+ channels of the lowest threshold found at the distal AIS and the regions distal to AIS corresponded to the low-threshold $Na_v1.6$ channels and those with higher threshold at the proximal AIS were largely the high-threshold $Na_v1.2$ channels[28] (**Figs. 1** and **3c**).

Modeling studies[35] have suggested that Na^+ channels may have cooperative activation, which may lead to a hyperpolarizing shift in their activation threshold. We examined this possibility by comparing the activation curves of Na^+ currents recorded in isolated axon blebs before and after partial blockade of Na^+ channels with tetrodotoxin (TTX), which decreases Na^+ currents by reducing the density of functional channels, a treatment that should diminish cooperative activation. Alternatively, we compared the activation of Na^+ currents in normal and low-Na^+ artificial cerebrospinal fluid (ACSF), which reduces the current amplitude without affecting the density of functional channels. As expected, we found that the peak amplitude of Na^+ currents was significantly reduced after puffing TTX (control, 1,389 ± 265 pA; TTX, 432 ± 166 pA; $P < 0.01$, $n = 8$) or in the presence of low-Na^+ ACSF (577 ± 60 pA, $P < 0.01$, $n = 9$) (**Fig. 4a,b**). We observed a slope change with TTX and in low-Na^+ ACSF (control, 3.6 ± 1.3; TTX, 5.3 ± 0.3; $P < 0.01$; low Na^+, 5.4 ± 0.2, $P < 0.01$), presumably as a result of better voltage clamp of small currents (**Supplementary Fig. 2**). However, there was no significant difference in the $V_{1/2}$ for both cases (control, −42.0 ± 0.7 mV; TTX, −42.1 ± 0.5 mV, $P = 0.95$; low Na^+, −41.8 ± 0.8 mV, $P = 0.82$; **Fig. 4c,d**), suggesting that cooperativity of channel opening does not contribute to the low threshold of axonal Na^+ channels that we observed under our experimental conditions.

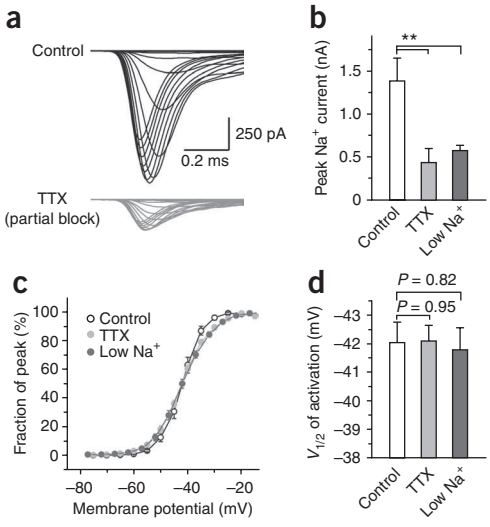

Figure 4 The low activation threshold of axonal Na^+ channels is not attributed to cooperative activation. (**a**) Representative families of currents recorded from an isolated bleb before and after puffing TTX (partially blocking Na^+ channels). (**b**) Average peak Na^+ currents in controls (open, $n = 8$), with TTX (gray, $n = 8$) and in low-Na^+ ACSF (black, $n = 9$). (**c**) Activation curves for Na^+ currents under these conditions. (**d**) Bar plot of $V_{1/2}$ in the three conditions (mean ± s.e.m.). ** indicates $P < 0.01$. Error bars represent s.e.m.

$Na_v1.6$ controls action potential initiation

We next used modeling analysis to investigate the role of Na^+ channel density and selective distribution of channel subtypes in action potential initiation and propagation. On the basis of our estimates of channel density and our immunostaining results (see Online Methods, **Fig. 5a** and **Supplementary Fig. 3**), our modeling analysis indicated that action potential initiation site is located at 40–45 μm from the soma, which is consistent with previous experimental findings[6,13,33]. Stepwise decreases in the total Na^+ channel density at the AIS from a value 40-fold to fivefold greater than that of soma resulted in a shift of the initiation site to a more distal location in the axon and an increase in the threshold current (or voltage, see Online Methods), with a rate of 0.023 nA (or 5.5 mV) per tenfold density decrease. Thus, the total Na^+ channel density at the AIS is critical for determining the location and threshold of action potential initiation.

To investigate the respective contribution of $Na_v1.6$ and $Na_v1.2$ channel density in determining the action potential initiation threshold, we constructed a model of the axon with uniform diameter and electrophysiological properties. Setting various combinations of $Na_v1.2$ and $Na_v1.6$ densities (from 80 to 3,000 pS μm^{-2}) resulted in action potential threshold changes. The contour lines of the action potential threshold changes largely paralleled the $Na_v1.2$ axis, but were perpendicular to the Nav1.6 density axis, indicating a predominant role of $Na_v1.6$, but not $Na_v1.2$, in determining the voltage threshold for action potential initiation (**Fig. 5b**). Plotting different combinations of channel subtype densities along the length of the AIS revealed that

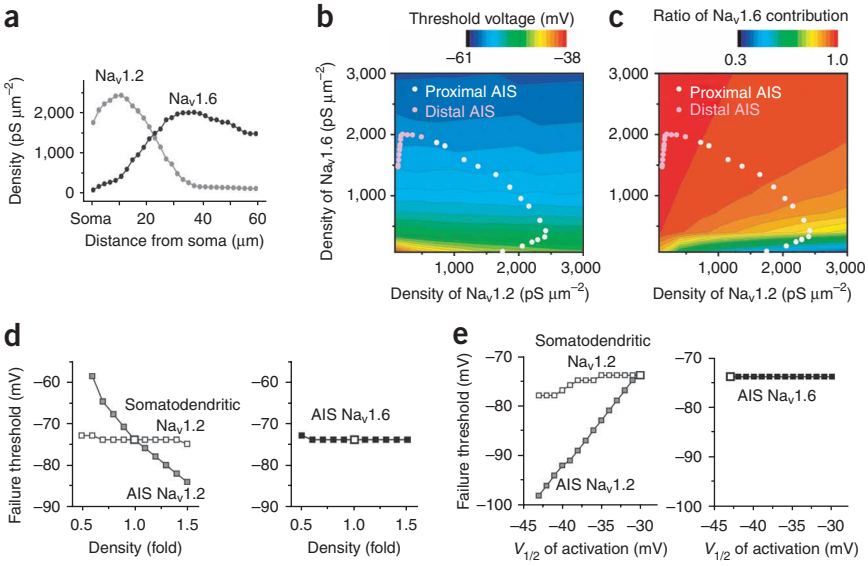

Figure 5 Simulations indicate distinct functions of AIS $Na_v1.6$ and $Na_v1.2$ in action potential initiation and backpropagation to the soma. (**a**) Density settings for $Na_v1.6$ and $Na_v1.2$ at the AIS based on experimental observations. (**b**) Contour map of the action potential threshold with various density combinations of the two channel subtypes. Dots indicate the local density for individual channel subtypes at the AIS (2-µm interval). (**c**) Contour map of the ratio of $Na_v1.6$-mediated conductance versus total Na^+ conductance at the action potential threshold. Dots indicate the local density for individual channel subtypes at the AIS (2-µm interval). (**d**) Plots of the failure threshold for somatic action potentials as a function of different density settings of the somatodendritic or AIS $Na_v1.2$ (left) and AIS $Na_v1.6$ (right). Backpropagating action potentials were evoked by current injection in axon regions distal to the AIS (**Supplementary Fig. 8**). (**e**) Dependence of the failure threshold on the voltage-dependent activation of the somatodendritic or AIS $Na_v1.2$ (left) and AIS $Na_v1.6$ (right).

the distal AIS had the lowest threshold (approximately −58 mV; **Fig. 5b**). Further calculation of the ratio of $Na_v1.6$-mediated conductance versus the total Na^+ conductance at the time of action potential initiation revealed a ratio close to 1 at the AIS beyond the first 10 µm (**Fig. 5c**). Together, these results indicate that the $Na_v1.6$ channels determine the lowest threshold of action potential initiation at the distal AIS. In contrast, the $Na_v1.2$ channels have a rather limited role in action potential initiation.

$Na_v1.2$ promotes action potential propagation to the soma

To examine how high-threshold perisomatic Na^+ channels affect the backpropagation of action potentials into the somatodendritic compartment, we performed modeling analysis (**Fig. 5d,e**) as well as simultaneous whole-cell recording from the soma and the axonal bleb (**Fig. 6a**). The generation of full somatic action potentials in response to axonal current injection depended on the level of somatic membrane potential (V_m; **Fig. 6b**). Close examination of the rising phase of the somatic action potentials revealed two components: the AIS and somatodendritic potential. Somatic spikelets (resulting from the arrival of AIS potentials) occurred frequently in response to axonal stimulation, reflecting the failure of somatodendritic potential (**Fig. 6b,c**). Plotting the probability of somatic action potential as a function of V_m revealed a steep voltage dependence, with an average V_m for the failure in action potential backpropagation (failure threshold) of −75.1 ± 2.4 mV ($n = 14$; **Fig. 6d**). The variability of this threshold may be attributed to the density variation of AIS $Na_v1.2$ channels among these neurons (see **Fig. 5**).

Consistent with these results, our simulations indicated that AIS $Na_v1.2$ channels are important in action potential backpropagation (**Fig. 5**). A decrease in the density of the $Na_v1.2$ channels at the AIS, but not of that in the somatodendritic compartment, resulted in a depolarizing shift in the failure threshold of action potential backpropagation to the soma, with a 2.8-mV shift per 10% density change (**Fig. 5d**). Complete removal of the AIS $Na_v1.2$ channels resulted in a decrease in the amplitude of somatic spikelets and caused a complete failure of action potential backpropagation (**Supplementary Fig. 4**). Setting hyperpolarizing $V_{1/2}$ of $Na_v1.2$ channels at the AIS (or somatodendritic compartments) from −30 to −43 mV resulted in a hyperpolarizing shift in the failure threshold with a rate of 1.8 mV per mV (or 0.3 mV per mV for somatodendritic compartment) (**Fig. 5e**). In contrast, the failure threshold was independent of the $V_{1/2}$ and the density of the AIS $Na_v1.6$ channels (**Fig. 5d,e**). Taken together, these results indicate that $Na_v1.2$ channels accumulated at the proximal AIS promote action potential backpropagation.

AIS and somatodendritic potential threshold

Our results suggest that both distal $Na_v1.6$ and proximal $Na_v1.2$ channels at the AIS are involved in generating full somatic action

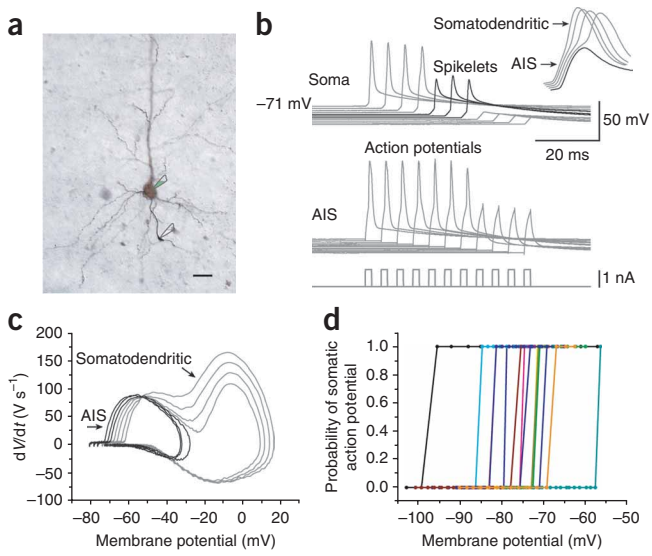

Figure 6 V_m dependence of action potential backpropagation. (**a**) Morphology of a recorded layer 5 pyramidal neuron in the prefrontal cortex. The two electrodes indicate the somatic and axonal recording sites. Scale bar represents 25 µm. (**b**) Simultaneous somatic and axonal recordings revealed that axonal action potentials evoked by current injection at the axon failed to generate full action potentials at hyperpolarizing somatic V_m. Note that only spikelets were detected at the soma when failure occurred. Inset, overlay of the somatic action potentials and one of the spikelets revealed two components, the AIS and somatodendritic potential. (**c**) Phase plots of the somatic action potentials and spikelets. (**d**) Plots of somatic action potential probability as a function of somatic V_m. Colored lines represent recordings from different neurons ($n = 14$).

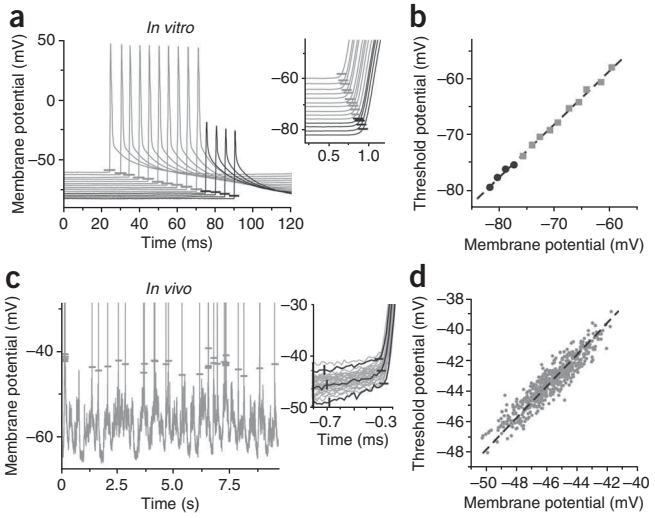

Figure 7 The threshold of somatic action potential is dependent on the preceding V_m. (**a**) Example sweeps from an *in vitro* recording (similar recording as in **Fig. 6**). Gray, full action potentials; black, spikelets (AIS potentials). Horizontal bars indicate the action potential thresholds. Inset, expansion of the action potential onset for clarity. (**b**) Threshold potentials of the action potentials (gray) and spikelets (black) in **a** are plotted as a function of V_m. The dashed line represents the linear regression fit. (**c**) An example trace of intracellular recording from a regular spiking neuron *in vivo*. Action potentials are truncated for clarity. Bars indicate the action potential thresholds. Inset, overlay of the onsets of all action potentials. Three individual traces are highlighted to show the correlation of action potential threshold and the level of V_m (vertical bars) at 0.4 ms before the threshold. (**d**) A plot of the threshold potential (from **c**) as a function of V_m ($n = 593$). The dashed line represents the linear regression fit.

potentials; activation of $Na_v1.6$ initiated the AIS potential, whereas activation of $Na_v1.2$ triggered the somatodendritic potential (**Fig. 6b,c**). Indeed, local application of TTX at the distal AIS markedly reduced the rising slope of the AIS potential, whereas similar application of TTX at the perisomatic region mostly affected the somatodendritic potential ($n = 12$; **Supplementary Fig. 5**). Further analysis showed that the AIS potential threshold measured at the soma (the traditional action potential threshold) correlated linearly with the somatic V_m (slope = 1.03 ± 0.04 mV per mV, $n = 14$, $r = 0.99$; **Fig. 7a,b**), suggesting that somatic V_m regulates the action potential threshold. This was further supported by the observation that action potentials generated at the active brain state, or the 'Up' state[36,37], had a threshold (−47.5 ± 0.1 mV, $n = 2254$ action potentials in seven regular spiking cells; **Fig. 7c,d**) that linearly correlated with V_m (slope = 0.93 ± 0.01 mV per mV; $r = 0.93$; **Fig. 7d**), suggesting that the highly variable threshold normally observed at the soma[35,38,39] may result from V_m fluctuations.

Because the somatodendritic potential is generated at the perisomatic region as a result of the activation of $Na_v1.2$ channels, somatic recording may faithfully reveal somatodendritic potential threshold, as suggested by a recent study[14], rather than AIS potential threshold. To further test this idea, we defined the somatodendritic potential threshold as the voltage at which the time derivative of V_m ($\frac{dV}{dt}$) is 20 V s^{-1} above the maximum curvature of the trough between the AIS and somatodendritic potentials in the phase plot (**Fig. 8a**). Consistent with recent estimates of the somatodendritic potential threshold[14], we found that the average threshold was −19.6 ± 4.8 mV ($n = 13$ cells), a value that was independent of the preceding V_m ($r = 0.12$),

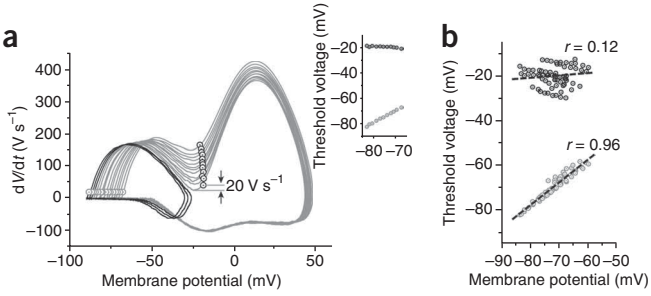

Figure 8 Voltage threshold of somatodendritic potential is independent of the preceding V_m. (**a**) Example phase plots of somatic action potentials (gray) and spikelets (black) evoked by current injection in the axon. Gray and black circles indicate the thresholds of the AIS potentials and the somatodendritic potentials, respectively. Inset, plot of the threshold voltage as a function of V_m. (**b**) Group results ($n = 13$). Gray, thresholds for AIS potentials; black, thresholds for somatodendritic potentials. Dashed lines indicate the best linear regression fits.

whereas AIS potential threshold showed a strong correlation with the V_m ($r = 0.96$, $n = 13$ cells; **Fig. 8b**).

These experimental data, together with simulation results, indicate that activation of $Na_v1.6$ channels at the distal AIS contributes to the determination of the AIS potential threshold, whereas activation of $Na_v1.2$ channels contributes to the determination of the somatodendritic potential threshold and thereby sets the threshold for the generation of full somatic action potentials.

DISCUSSION

In this study, we found that $Na_v1.2$ and $Na_v1.6$ are selectively targeted to the proximal and distal AIS, respectively. The distribution of $Na_v1.6$ channel peaked at the distal AIS, corresponding to the action potential initiation zone. Consistently, our electrophysiological experiments indicated that Na^+ channels at the distal AIS and the adjacent axon had a lower activation threshold than those at the proximal AIS and the soma. Moreover, our regular and giant patch recordings provide direct evidence that AIS has a higher Na^+ current density than the soma and nearby axon regions, with a ratio of 1 to 34 to 27 (soma to AIS to adjacent axon). Our simulation results further support the notion that $Na_v1.6$ channels accumulated at the distal AIS determine the lowest threshold for action potential initiation. The results of our simultaneous somatic and axonal recordings, together with simulations, indicate that the highly clustered $Na_v1.2$ channels at the proximal AIS strongly promote, if not guarantee, action potential backpropagation into the soma.

Density and activation threshold of axonal Na^+ channels

Previous outside-out patch recordings from AIS of pyramidal neurons have suggested that the Na^+ channel density is up to threefold greater than that of the soma[3]. However, a recent study[23] has demonstrated that the channel density may be underestimated as a result of tight channel anchoring to the intracellular cytoskeleton. We found that the peak amplitudes of Na^+ currents recorded from the axonal patches were significantly higher than those of the somatic ones ($P < 0.001$; **Fig. 2**), consistent with previous immunostaining results[12,18,19,25,34] and computational predictions[4,17]. Although we obtained recordings from injured axons, several lines of evidence indicate that these density estimates are likely to reflect the actual density in the axon. First, our immunostaining revealed similar signal levels at the axon trunk versus terminal bleb (**Supplementary Fig. 6**). Second, axonal action potentials recorded at the bleb had a profile similar to those recorded at the AIS,

with a rapid rising phase reflecting the high availability of Na^+ channels[39]. Third, axonal Na^+ channels may be freed from the tight association with cytoskeleton during the slicing procedure. Immunoreactivity for AnkG was undetectable in the axon blebs ($n = 25$ of 25; **Supplementary Fig. 6**). Finally, our giant patch recording made from the isolated blebs as a whole had minimized the influence of tight channel anchoring to the cytoskeleton and yielded results similar to those from outside-out patches (**Fig. 2**). Together, our results provide, to the best of our knowledge, the first direct electrophysiological evidence of a high Na^+ channel density at the AIS and the regions beyond the AIS.

Differential biophysical properties of Na^+ channels along the somato-axonal axis may result from a differential distribution of channel subtypes[18], different levels of phosphorylation[40] and density-dependent cooperative activation[35]. Previous work has revealed that $Na_v1.6$ channels are activated and inactivated at more negative V_m than $Na_v1.2$ channels[28]. Here, we found that the selective accumulation of $Na_v1.2$ and $Na_v1.6$ channels at the proximal and distal AIS correlated directly with the reduction in $V_{1/2}$ (**Fig. 3**). A recent study[24] found a gradual increase in $Na_v1.6$ immunostaining intensity at the AIS in layer 2/3, but not in layer 5 pyramidal cells. In contrast, our experiments revealed a nonuniform distribution of $Na_v1.6$ at the AIS of layer 5 pyramidal neurons in both the prefrontal cortex and the primary somatosensory cortex (**Supplementary Fig. 7**). Whether these differences in immunostaining results could be attributed to regional differences in the brain remains unknown.

The notion of cooperative channel activation[35], whereby the opening of a Na^+ channel lowers the activation threshold of its neighboring channels in a distance-dependent manner, was excluded by partial TTX blockade and low-Na^+ experiments. Application of TTX should diminish the cooperative activation of Na^+ channels by increasing the distance between functional channels, whereas application of low-Na^+ ACSF would not change the channel cooperativity because the density of functional channels were not affected. However, we found no substantial change in the $V_{1/2}$ with either treatment (**Fig. 4**). Therefore, we conclude that preferential distribution and clustering of Na^+ channel subtypes represent the predominant factors in determining the low threshold of action potential initiation at the AIS. Whether differential channel phosphorylation in subcellular compartments may also contribute to the activation threshold remains to be examined.

Distinct functions of $Na_v1.6$ and $Na_v1.2$

Previous computational studies have yielded conflicting conclusions about the role of Na^+ channel density and biophysical properties in action potential initiation as a result of inconsistent estimates of channel density[3,4,17,23]. Our modeling studies integrated the immunostaining and electrophysiological results and showed that the lowest threshold for action potential initiation at the distal AIS was largely determined by the density of low-threshold $Na_v1.6$ channels (**Fig. 5**). Consistent with these modeling results, axonal $Na_v1.6$ channels have been shown to lower the threshold voltage and participate in action potential initiation in different neuronal types[1,2,26].

Distinct from the function of $Na_v1.6$ channel, the $Na_v1.2$ channel may control action potential backpropagation because of its high density at the proximal AIS and high threshold. Our simulations revealed a depolarizing shift of the failure threshold for action potential backpropagation with a decreasing density of the AIS $Na_v1.2$ channels (**Fig. 5d**). Removal of these channels resulted in a decrease in the spikelet amplitude and a complete failure of action potential backpropagation (**Supplementary Fig. 4**). Experimental (**Fig. 6**) and modeling results (**Fig. 5e**) indicate that somatic invasion of backpropagating action potentials is tightly linked to the somatic V_m and voltage-dependent activation of AIS $Na_v1.2$ channels. Consistent with a recent study[14], our experiments revealed a threshold of approximately −20 mV for somatodendritic potentials, and further demonstrated that this threshold, but not that of AIS potential recorded at the soma, remained constant in accordance with somatic V_m fluctuations. Because successful invasion of the backpropagating action potential into the dendritic tree is critical for synaptic plasticity[7,41–45], $Na_v1.2$ channels at AIS may participate in neuronal plasticity.

In conclusion, distal AIS accumulation of $Na_v1.6$ channels determines the low threshold for action potential initiation; whereas proximal AIS accumulation of $Na_v1.2$ channels sets the threshold for the generation of somatodendritic potentials and ensures action potential backpropagation to the soma and dendrites. Thus, $Na_v1.6$ and $Na_v1.2$ channels serve distinct functions in action potential initiation and backpropagation.

METHODS

Methods and any associated references are available in the online version of the paper at http://www.nature.com/natureneuroscience/.

Note: Supplementary information is available on the Nature Neuroscience website.

ACKNOWLEDGMENTS

We thank M.M. Poo, D.A. McCormick and M.H. Kole for their valuable comments on this work. We are also grateful to Y. Yu for his help in computer modeling. This work was supported by the 973 Program (2006CB806600), a Shanghai Commission of Science and Technology grant (06DJ14010), the Shanghai Pujiang Program (07PJ14108), the Hundreds of Talents Program and Knowledge Innovation Project from Chinese Academy of Sciences (KSCX2-YW-R-102), and Projects of the Scientific Research Foundation of the State Human Resource Ministry and the Education Ministry.

AUTHOR CONTRIBUTIONS

W.H. performed the patch-clamp and whole-cell recording experiments, simulations, and data analysis. C.T. carried out the immunostaining experiments. T.L. performed the sharp electrode recordings. M.Y. and H.H. helped with data analysis and simulations. Y.S. designed the experiments and wrote the paper.

Published online at http://www.nature.com/natureneuroscience/.
Reprints and permissions information is available online at http://www.nature.com/reprintsandpermissions/.

1. Clark, B.A., Monsivais, P., Branco, T., London, M. & Hausser, M. The site of action potential initiation in cerebellar Purkinje neurons. *Nat. Neurosci.* **8**, 137–139 (2005).
2. Colbert, C.M. & Johnston, D. Axonal action-potential initiation and Na^+ channel densities in the soma and axon initial segment of subicular pyramidal neurons. *J. Neurosci.* **16**, 6676–6686 (1996).
3. Colbert, C.M. & Pan, E. Ion channel properties underlying axonal action potential initiation in pyramidal neurons. *Nat. Neurosci.* **5**, 533–538 (2002).
4. Mainen, Z.F., Joerges, J., Huguenard, J.R. & Sejnowski, T.J. A model of spike initiation in neocortical pyramidal neurons. *Neuron* **15**, 1427–1439 (1995).
5. Milojkovic, B.A., Wuskell, J.P., Loew, L.M. & Antic, S.D. Initiation of sodium spikelets in basal dendrites of neocortical pyramidal neurons. *J. Membr. Biol.* **208**, 155–169 (2005).
6. Stuart, G., Schiller, J. & Sakmann, B. Action potential initiation and propagation in rat neocortical pyramidal neurons. *J. Physiol. (Lond.)* **505**, 617–632 (1997).
7. Stuart, G., Spruston, N., Sakmann, B. & Hausser, M. Action potential initiation and backpropagation in neurons of the mammalian CNS. *Trends Neurosci.* **20**, 125–131 (1997).
8. Coombs, J.S., Curtis, D.R. & Eccles, J.C. The interpretation of spike potentials of motoneurones. *J. Physiol. (Lond.)* **139**, 198–231 (1957).
9. Eccles, J.C. *The Physiology of Nerve Cells* (The Johns Hopkins Press, Baltimore, 1957).
10. Fatt, P. Sequence of events in synaptic activation of a motoneurone. *J. Neurophysiol.* **20**, 61–80 (1957).
11. Fuortes, M.G., Frank, K. & Becker, M.C. Steps in the production of motoneuron spikes. *J. Gen. Physiol.* **40**, 735–752 (1957).
12. Meeks, J.P. & Mennerick, S. Action potential initiation and propagation in CA3 pyramidal axons. *J. Neurophysiol.* **97**, 3460–3472 (2007).
13. Shu, Y., Duque, A., Yu, Y., Haider, B. & McCormick, D.A. Properties of action-potential initiation in neocortical pyramidal cells: evidence from whole cell axon recordings. *J. Neurophysiol.* **97**, 746–760 (2007).
14. Kole, M.H. & Stuart, G.J. Is action potential threshold lowest in the axon? *Nat. Neurosci.* **11**, 1253–1255 (2008).

15. Dodge, F.A. & Cooley, J.W. Action potential of the motoneuron. *IBM J. Res. Develop.* **17**, 219–229 (1973).
16. Moore, J.W., Stockbridge, N. & Westerfield, M. On the site of impulse initiation in a neurone. *J. Physiol. (Lond.)* **336**, 301–311 (1983).
17. Rapp, M., Yarom, Y. & Segev, I. Modeling back propagating action potential in weakly excitable dendrites of neocortical pyramidal cells. *Proc. Natl. Acad. Sci. USA* **93**, 11985–11990 (1996).
18. Van Wart, A., Trimmer, J.S. & Matthews, G. Polarized distribution of ion channels within microdomains of the axon initial segment. *J. Comp. Neurol.* **500**, 339–352 (2007).
19. Inda, M.C., DeFelipe, J. & Munoz, A. Voltage-gated ion channels in the axon initial segment of human cortical pyramidal cells and their relationship with chandelier cells. *Proc. Natl. Acad. Sci. USA* **103**, 2920–2925 (2006).
20. Kole, M.H., Letzkus, J.J. & Stuart, G.J. Axon initial segment Kv1 channels control axonal action potential waveform and synaptic efficacy. *Neuron* **55**, 633–647 (2007).
21. Shu, Y., Yu, Y., Yang, J. & McCormick, D.A. Selective control of cortical axonal spikes by a slowly inactivating K^+ current. *Proc. Natl. Acad. Sci. USA* **104**, 11453–11458 (2007).
22. Howard, A., Tamas, G. & Soltesz, I. Lighting the chandelier: new vistas for axo-axonic cells. *Trends Neurosci.* **28**, 310–316 (2005).
23. Kole, M.H. *et al.* Action potential generation requires a high sodium channel density in the axon initial segment. *Nat. Neurosci.* **11**, 178–186 (2008).
24. Lorincz, A. & Nusser, Z. Cell type–dependent molecular composition of the axon initial segment. *J. Neurosci.* **28**, 14329–14340 (2008).
25. Boiko, T. *et al.* Functional specialization of the axon initial segment by isoform-specific sodium channel targeting. *J. Neurosci.* **23**, 2306–2313 (2003).
26. Royeck, M. *et al.* Role of axonal Nav1.6 sodium channels in action potential initiation of CA1 pyramidal neurons. *J. Neurophysiol.* **100**, 2361–2380 (2008).
27. Duflocq, A., Le Bras, B., Bullier, E., Couraud, F. & Davenne, M. Nav1.1 is predominantly expressed in nodes of Ranvier and axon initial segments. *Mol. Cell. Neurosci.* **39**, 180–192 (2008).
28. Rush, A.M., Dib-Hajj, S.D. & Waxman, S.G. Electrophysiological properties of two axonal sodium channels, Nav1.2 and Nav1.6, expressed in mouse spinal sensory neurones. *J. Physiol. (Lond.)* **564**, 803–815 (2005).
29. Boiko, T. *et al.* Compact myelin dictates the differential targeting of two sodium channel isoforms in the same axon. *Neuron* **30**, 91–104 (2001).
30. Kaplan, M.R. *et al.* Differential control of clustering of the sodium channels Na(v)1.2 and Na(v)1.6 at developing CNS nodes of Ranvier. *Neuron* **30**, 105–119 (2001).
31. Komai, S. *et al.* Postsynaptic excitability is necessary for strengthening of cortical sensory responses during experience-dependent development. *Nat. Neurosci.* **9**, 1125–1133 (2006).
32. Shu, Y., Hasenstaub, A., Duque, A., Yu, Y. & McCormick, D.A. Modulation of intracortical synaptic potentials by presynaptic somatic membrane potential. *Nature* **441**, 761–765 (2006).
33. Palmer, L.M. & Stuart, G.J. Site of action potential initiation in layer 5 pyramidal neurons. *J. Neurosci.* **26**, 1854–1863 (2006).
34. Wollner, D.A. & Catterall, W.A. Localization of sodium channels in axon hillocks and initial segments of retinal ganglion cells. *Proc. Natl. Acad. Sci. USA* **83**, 8424–8428 (1986).
35. Naundorf, B., Wolf, F. & Volgushev, M. Unique features of action potential initiation in cortical neurons. *Nature* **440**, 1060–1063 (2006).
36. Shu, Y., Hasenstaub, A. & McCormick, D.A. Turning on and off recurrent balanced cortical activity. *Nature* **423**, 288–293 (2003).
37. Steriade, M., Nunez, A. & Amzica, F. A novel slow (<1 Hz) oscillation of neocortical neurons in vivo: depolarizing and hyperpolarizing components. *J. Neurosci.* **13**, 3252–3265 (1993).
38. Yu, Y., Shu, Y. & McCormick, D.A. Cortical action potential backpropagation explains spike threshold variability and rapid-onset kinetics. *J. Neurosci.* **28**, 7260–7272 (2008).
39. McCormick, D.A., Shu, Y. & Yu, Y. Neurophysiology: Hodgkin and Huxley model—still standing? *Nature* **445**, E1–2; discussion E2–3 (2007).
40. Colbert, C.M. & Johnston, D. Protein kinase C activation decreases activity-dependent attenuation of dendritic Na^+ current in hippocampal CA1 pyramidal neurons. *J. Neurophysiol.* **79**, 491–495 (1998).
41. Bi, G.Q. & Poo, M.M. Synaptic modifications in cultured hippocampal neurons: dependence on spike timing, synaptic strength and postsynaptic cell type. *J. Neurosci.* **18**, 10464–10472 (1998).
42. Kampa, B.M., Clements, J., Jonas, P. & Stuart, G.J. Kinetics of Mg^{2+} unblock of NMDA receptors: implications for spike timing–dependent synaptic plasticity. *J. Physiol. (Lond.)* **556**, 337–345 (2004).
43. Kampa, B.M., Letzkus, J.J. & Stuart, G.J. Requirement of dendritic calcium spikes for induction of spike timing–dependent synaptic plasticity. *J. Physiol. (Lond.)* **574**, 283–290 (2006).
44. Markram, H., Lubke, J., Frotscher, M. & Sakmann, B. Regulation of synaptic efficacy by coincidence of postsynaptic APs and EPSPs. *Science* **275**, 213–215 (1997).
45. Sjöström, P.J., Turrigiano, G.G. & Nelson, S.B. Rate, timing, and cooperativity jointly determine cortical synaptic plasticity. *Neuron* **32**, 1149–1164 (2001).

ONLINE METHODS

Slice preparation. We obtained coronal slices of the prefrontal cortex from P16–20 Sprague-Dawley rats. The use and care of the rats complied with the guidelines of the Animal Advisory Committee at the Shanghai Institutes for Biological Sciences. We anesthetized the rats deeply with sodium pentobarbital (30 mg per kg of body weight) and then quickly dissected out the brain and placed it in ice-cold, oxygenated (95% O_2 and 5% CO_2), sucrose-substituted ACSF in which equiosmolar sucrose was used as a substitute for NaCl. In this solution, we cut the slices (300 μm) with a microtome (VT1000S, Leica) and incubated them in aerated normal ACSF containing 125 mM NaCl, 2.5 mM KCl, 2 mM $MgSO_4$, 2 mM $CaCl_2$, 26 mM $NaHCO_3$, 1.25 mM NaH_2PO_4 and 25 mM dextrose (315 mOsm, pH 7.4, 35 °C). After ~45 min of incubation, we transferred the slices to a chamber bathed with aerated ACSF (36–36.5 °C) and visualized the cortical neurons with an upright infrared differential interference contrast microscope (BX51WI, Olympus).

Electrophysiological recordings. In this study, we used a new method of patch recording from the cut end of the axon to probe the ion channels at the AIS and the axon[13,21,32]. We performed patch-clamp and whole-cell recordings from layer 5 pyramidal neurons with a Multiclamp 700B or an Axopatch 200B amplifier (Molecular Devices). Patch pipettes had an impedance of 5–7 MΩ with an internal solution containing 145 mM CsCl, 2 mM $MgCl_2$, 2 mM Na_2ATP, 10 mM HEPES, 0.2 mM EGTA and 2 mM TEA (tetraethylammonium) (pH 7.2 with CsOH, 287 mOsm). To trace and label the recorded neurons, we added Alexa Fluor 488 (100 μM) and biocytin (0.2%) to the pipette solution. The pipettes that we used for regular somatic and axonal outside-out patch recordings were made with the same protocol in the puller and had similar impedance. To isolate the Na^+ currents, we added $CdCl_2$ (200 μM) to the bath solution and TEA to the Cs^+-based internal solution. We recorded Na^+ currents from regular outside-out patches excised from the soma and the axon blebs, and also from giant outside-out patches: the somatic nucleated patches[46] and the isolated axon blebs. We obtained the axon blebs by sweeping a sharp electrode underneath the slice surface at the border of layer 6 and white matter (to disconnect the bleb and the main axon). Bath application of 1 μM TTX could completely block the somatic and axonal inward currents.

We recorded families of Na^+ currents in response to serials of depolarizing voltage steps (30 ms) from a preceding prepulse of −100 (50 ms) to +20 mV and generated the activation curves on the basis of the peak currents at each step. Activation threshold of the Na^+ currents was the voltage at which the evoked peak current reached 10% of the maximum value. We plotted the inactivation curves using the peak currents elicited by a test pulse (30 ms) to −5 mV following a range of voltage steps (50 ms) from −115 to −5 mV. We calculated the current density of a certain giant patch by dividing the peak current (evoked during the activation protocols) by membrane area (obtained by carefully measuring the diameter of the nucleated patches and isolated axon blebs). The current density was measured at −5 mV and −20 mV for somatic and axonal patches, respectively. To test the voltage dependence of axonal Na^+ channels with reduced density, we put a glass pipette filled with TTX (50 μM) upstream of the perfusion flow to obtain a peak current less than one-third of the original amplitude (**Fig. 4**). In contrast, we bathed the slice with a low-Na^+ ACSF (67% NaCl was replaced with NMDG) to reduce the peak current, but leave all channels available for activation. We obtained simultaneous somatic and axonal recording in normal ACSF with patch pipettes filled with K^+-based internal solution (140 mM potassium gluconate, 3 mM KCl, 2 mM $MgCl_2$, 2 mM Na_2ATP, 10 mM HEPES and 0.2 mM EGTA, pH 7.2 with KOH, 288 mOsm).

For *in vivo* recordings, we initially anesthetized the rats (280–350 g) with urethane (1.0 g per kg, intraperitoneal) and supplemented with ketamine and xylazine hourly (35 mg per kg and 7 mg per kg, respectively, intramuscular). We performed intracellular recordings from cortical regular spiking neurons with an AxoClamp 2B amplifier (Molecular Devices). Sharp electrodes had an impedance of 60–90 MΩ filled with 2 M potassium acetate.

Our somatic and axonal recordings had an access resistance of less than 20 and 25 MΩ, respectively. We digitally subtracted the leakage currents using an on-line P/5 procedure (in which the currents evoked by five hyperpolarizing pulses with one-fifth amplitude of the test pulse P were summed and added to the current trace of interest) and low-pass filtered the currents at 10 kHz and sampled at 100 kHz using pClamp 10 software and a Digidata 1440A interface (Molecular Devices). The V_m values shown in the text and figures were corrected with calculated liquid junctions for different internal solutions.

Statistical analysis. Data are presented as mean ± s.e.m. Statistical tests were performed using two-tailed Student's *t* test.

Immunostaining. We killed the rats by perfusion with 1% paraformaldehyde and 1% sucrose (wt/vol) in 0.1 M phosphate buffer (pH 7.4) after deep anesthesia with sodium pentobarbital. The brain was removed and post-fixed in the same fixative for 2 h and then immersed in 30% sucrose in 0.1 M phosphate buffer for 48 h. We obtained cryostat coronal sections (16 or 100 μm) using a freezing microtome. In some experiments, we also used slices (300 μm) prepared for electrophysiological recordings.

We rinsed the sections in 0.01 M phosphate-buffered saline (PBS, pH 7.4) and incubated them in a blocking solution (5% normal goat serum, 0.3% Triton X-100 in PBS, vol/vol) at 20–25 °C for 2 h. Sections were incubated overnight at 4 °C with primary antibody to AnkG (1:200, Santa Cruz) and either $Na_v1.2$, $Na_v1.6$ or Pan-Na_v (1:200, Alomone) in 0.1% Triton (vol/vol). After a complete wash in PBS, these sections were incubated in Alexa 488–conjugated goat antibody to rabbit IgG and Alexa 594 goat antibody to mouse IgG in 0.1% Triton (1:1,000; Molecular Probes) at 20–25 °C for 2 h. We then washed and mounted the sections with Vecta shield mounting media (Vector Laboratories). We took images in the linear range of the photomultiplier with a laser scanning confocal microscope (ZEISS LSM 510 META NLO) and used the projection of *z* stack images (0.4 μm per image) in the figures. We did not detect labeling in the controls (not treated with primary antibodies).

We then used Autoquant X2 software (Media Cybernetics) to deconvolve the images and employed Amira software (Mercury Computer Systems) to extract axon signals and measure the fluorescence intensity. Briefly, we subtracted the background (mean fluorescence intensity of the stack) from the deconvolved image and obtained an image named C1, and then generated two masks from this image (for Na^+ channel staining and AnkG staining) by defining an intensity threshold of mean ± 3 s.d. We applied an OR operation of the masks and obtained a mask image called C2, and then applied an AND operation of C1 and C2 to obtain the image C3, in which only axonal profiles were kept. In C2, we traced the axons (total volume >5,000 voxels) and got an axon line set. Short axons and those with truncated axon hillock were discarded. We measured the axon diameter in C2 and sampled the fluorescence values in C3 on the basis of the line set. The fluorescence intensities were normalized to the peak value at the AIS and averaged between different axons.

Model construction. We implemented two new voltage-gated Na^+ channels, nasoma and naaxon, whose properties were described by Hodgkin-Huxley–style equations[4,47], to simulate the channels at the soma and the distal AIS, respectively. The parameters of nasoma and naaxon were initially set to the experimentally observed values (**Fig. 3**). We inserted the two channels (gbar = 100 pS μm^{-2}) into a single compartment model (length, 10 μm; diameter, 10 μm) to examine their voltage-dependent properties (**Supplementary Fig. 3**).

The computational model was implemented using NEURON 6 (ref. 48) and a previously published multicompartmental model of the full dendritic and somatic structure of a layer 5 cortical pyramidal cell[49] coupled with a cylindrical AIS and axon segments[32,38]. The main axon started with an axon hillock (length, 10 μm) that connected to the soma and tapered from a diameter of 3.8 to 2.4 μm, followed by an AIS (length, 50 μm; diameter, 1.22 μm). The AIS was attached by an unmyelinated axon (length, 400 μm; diameter, 1.02 μm) and then a myelinated axon (400 μm in length) with internode distances of 100 μm. The electrical properties R_m, C_m and R_i were set to 30,000 Ω cm^2, 1 μF cm^{-2} and 150 Ω cm, respectively, and distributed uniformly throughout the cell. Myelination was simulated by reducing C_m to 0.02 μF cm^{-2}. The resting V_m at soma was set to −70 mV. All simulations were run with 20-μs time steps and the nominal temperature of simulation was 37 °C.

The transient Na^+ current was present in all parts of the model cell, but the channel subtypes were nonuniformly distributed according to our experimental observations. Specifically, nasoma was present in soma, dendrites and proximal AIS, whereas naaxon was present in proximal AIS, but dominant in distal AIS and the axon regions distal to AIS (**Fig. 5a**). From the recordings of nucleated

patches, we obtained an average channel density of 45.6 ± 3.7 pS μm^{-2} (16–107 pS μm^{-2}, corrected with a maximum open probability of 0.5, $n = 34$)[50]. Considering that this density might be underestimated as a result of membrane stretching and that a density of 80 pS μm^{-2} (which was in the range of our estimates) in the dendrite and soma has been found by previous studies[50], we therefore set a density of 80 pS μm^{-2} for the somatodendritic compartments as a starting point of the simulations. Reducing channel density to 60 and 45 pS μm^{-2} for somatic and dendritic compartments, respectively, yielded similar results. Unless otherwise stated, channel density was set to 300 pS μm^{-2} in the axon regions distal to the AIS (>60 μm) and 1,600 pS μm^{-2} in the nodes of Ranvier. At the AIS, nasoma and naaxon contributed to the total channel density according to immunostaining results with a maximum density of 3,200 pS μm^{-2} (40-fold greater than that in soma). The Na^+ equilibrium potential was set to +60 mV.

The fast voltage-gated K^+ current, I_{Kv}, was present in the soma (20 pS μm^{-2}), dendrites (10 pS μm^{-2}) and unmyelinated axon (1,500 pS μm^{-2}). It increased linearly with distance in the AIS to a maximum value of 1,000 pS μm^{-2}. The K^+ equilibrium potential was set to −90 mV. The slow non-inactivating potassium current (M current; I_{km}), high-voltage activated Ca^{2+} current (I_{Ca}) and Ca^{2+}-dependent K^+ current (I_{kCa}) were distributed throughout the somatic and dendritic compartments and had conductances of 0.3, 0.3 and 3 pS μm^{-2}, respectively. Background leak conductance (gleak) was distributed throughout the cell with a density of 0.33 pS μm^{-2}, except for the nodes of Ranvier (200 pS μm^{-2}). The reversal potential of the leak current was −70 mV.

The action potential initiation site was defined as the location where the $\frac{dV}{dt}$ first reached 20 V s^{-1}. The threshold voltage was defined as the somatic V_m at which $\frac{dV}{dt}$ reached 20 V s^{-1}, whereas the threshold current was the minimum amount of current (duration, 100 ms) injected into the soma to evoke a single action potential.

46. Sather, W., Dieudonne, S., MacDonald, J.F. & Ascher, P. Activation and desensitization of N-methyl-D-aspartate receptors in nucleated outside-out patches from mouse neurones. *J. Physiol. (Lond.)* **450**, 643–672 (1992).
47. Hodgkin, A.L. & Huxley, A.F. A quantitative description of membrane current and its application to conduction and excitation in nerve. *J. Physiol. (Lond.)* **117**, 500–544 (1952).
48. Hines, M.L. & Carnevale, N.T. The NEURON simulation environment. *Neural Comput.* **9**, 1179–1209 (1997).
49. Mainen, Z.F. & Sejnowski, T.J. Influence of dendritic structure on firing pattern in model neocortical neurons. *Nature* **382**, 363–366 (1996).
50. Engel, D. & Jonas, P. Presynaptic action potential amplification by voltage-gated Na^+ channels in hippocampal mossy fiber boutons. *Neuron* **45**, 405–417 (2005).

doi:10.1038/nn.2359